

Nanoconfined (bio)catalysts as efficient glucose-responsive nanoreactors

*Andoni Rodriguez-Abetxuko, Pablo Muñumer, Mitsuhiro Okuda, Javier Calvo, Mato Knez, Ana Beloqui**

A.R.-A.

CICnanoGUNE, Av. Tolosa, 76, E-20018 Donostia - San Sebastian (Spain)

P.M.

CICnanoGUNE, Av. Tolosa, 76, E-20018 Donostia - San Sebastian (Spain)

POLYMAT-UPV/EHU, Avda. Manuel de Lardizabal 3, E-20018 Donostia - San Sebastian, (Spain)

Dr. M.O. and Prof. M. K.

CICnanoGUNE, Av. Tolosa, 76, E-20018 Donostia - San Sebastian (Spain)

IKERBASQUE, Basque Foundation for Science, Maria Diaz de Haro 3, E-48013 Bilbao (Spain)

Dr. J.C.

CICbiomaGUNE, Paseo Miramón, 182, E-20009 Donostia - San Sebastian (Spain)

Dr. A.B.

POLYMAT-UPV/EHU, Avda. Manuel de Lardizabal 3, E-20018 Donostia - San Sebastian, (Spain)

IKERBASQUE, Basque Foundation for Science, Maria Diaz de Haro 3, E-48013 Bilbao (Spain)

E-mail: ana.beloquie@ehu.eus

Keywords: chemoenzymatic nanoreactors, responsive nanomaterials, cascade reaction, artificial metabolic channels, biodegradation of aromatics

Herein we show the design, synthesis, and characterization of bifunctional hybrid nanoreactors used for concurrent one-pot chemoenzymatic reactions. In our design, the enzyme, glucose oxidase, is wrapped with a peroxidase-mimetic catalytic polymer. Hemin, the organic catalyst, is linked to the flexible polymeric scaffold through coordination to the imidazole groups that hang out the network. This spatial arrangement, that works as a metabolic channel, is optimized for cooperative chemoenzymatic reactions in which the enzyme catalyzes first. A deep characterization of the integrated nanoreactors has demonstrated that the confinement of two distinct catalytic sites in the nanospace is very effective in one-pot reactions. Moreover, besides its role as scaffold material, the polymeric mantle protects both the biocatalyst and the chemical catalyst from degradation and inactivation in presence of organic solvents. Furthermore, the

polymeric environment of the nanoreactors can be tailored in order to trigger the assembly of those into highly active heterogeneous hybrid catalysts. Finally, we have applied our new nanoreactors to the efficient degradation of organic aromatic compounds using glucose as the only fuel.

1. Introduction

The design of new hybrid nanostructures which integrate two or more connected functions into a single entity are sought for further advances in the development of nanomaterials for biosensing and chemical applications.^[1,2] Certainly, the close-positioning and the correct spatial arrangement of distinct functional, i.e. catalytic, units into a confined volume at the nanoscale, resembling metabolic channels in cells, is beneficial for the development of one-pot reactions within the hybrid complex.^[3–5] Compared to step-wise catalysis, sequential reactions usually show a cooperative effect that improves the overall synthetic performance of the reaction.^[6] However, while the combination of bio- and chemocatalysts has proven successful in chemical synthesis,^[7] their joint utilization as chemoenzymatic one-pot reactors becomes scientifically challenging due to operational limitations related to the incompatibility and the mutual inactivation of the catalysts.^[8–11] Moreover, there are only few methods available to proceed with the confinement of (bio)catalysts and to fabricate artificial complexes in a controlled manner.

In our aim at building highly efficient chemoenzymatic nanoreactors, we sought for an appropriate scaffold material that accommodates and protects the enzyme and the organic catalyst from inactivation. In this regard, the flexibility and permeability of polymers are attractive in order to recreate three-dimensional architectures that are sought for hybrid nanoreactors.^[12] Moreover, a convenient arrangement of the catalysts that could foster the efficiency of cascade reactions in a small volume is preferred.^[13]

These demands can be fulfilled using enzyme nanogels synthesized with functional polymers. In our group, we have successfully wrapped single enzymes with a functional polymeric network using the single enzyme nanogel (SEN) synthesis approach. SENs are polymeric nanogels that are filled with single proteins.^[14] A thin polymeric shell is pursued to minimize the substrate/product diffusion issues while improving the protection of the inner protein against denaturation under harsh conditions such as high temperatures or presence of solvents.^[15] Furthermore, the design of polymeric mantels with functional groups, i.e. imidazole, can be used to distribute the organic catalyst along the shell, encircling the enzyme, through metal-ligand coordination.^[16–18] Thus, in contrast to other reported sequentially arrayed chemoenzymatic systems, our approach involves a core-shell positioning of the catalysts, which is particularly beneficial for tandem reactions in which the enzyme works first.

In this work, we present a new and general method to tether and localize hemin molecules, as chemical catalyst, throughout the polymeric shell of the imidazole-decorated single enzyme nanogels of glucose oxidase (GOx). The catalytic features of the hemin complex are interesting for both its ability to catalyze small molecules and its planar structure that can be easily bound to several 3D and 2D materials. Hence, diverse materials such as graphene oxide, clay, zeolites, MOFs, gold nanowires, and biomacromolecules such as G-quadruple DNA have been used as supports for iron porphyrin molecules for the fabrication of functional materials with peroxidase-like activity.^[19,20] In most of the reported hybrid materials, hemin is linked through the side groups, i.e. carboxylic or vinyl groups. However, given the fact that a strong influence of the nature of the coordinating ligands on the performance of hemin catalysts exists,^[21,22] an adequate accommodation of hemin molecules within the supramolecular materials is of great importance. Therefore, with the utilization of imidazole-decorated

nanogels, we target at mimicking peroxidase enzymes, in which the link of the hemin molecule to histidine residues, namely imidazole ligands, boosts the catalytic activity drastically.^[23,24]

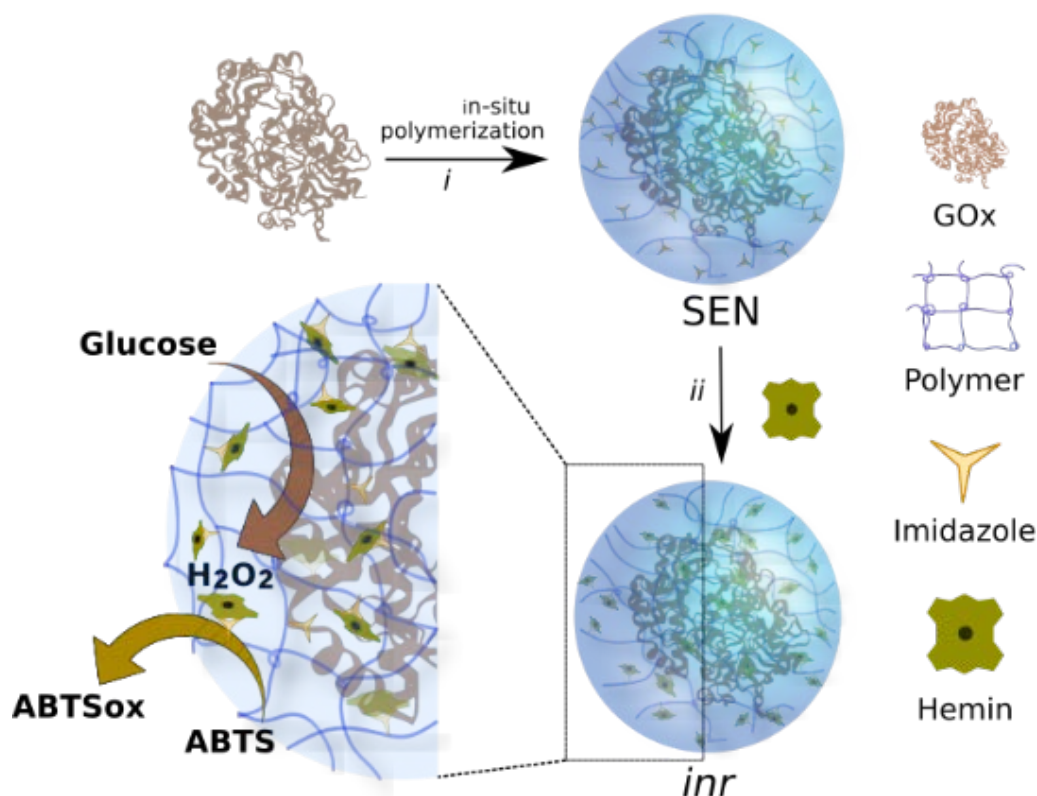
Finally, great effort is being invested for the development of an effective peroxidation system for the degradation of organic compounds.^[25,26] Both phenolic derivatives and organic dyes, which are usually poured into wastewater by textile and paper industries, are known to be threatening for human health and aquatic living organisms.^[27] Most of the (bio)chemical peroxidation systems designed for the decomposition of aromatic compounds are based on the use of relatively high concentrations of hydrogen peroxide as peroxidation agent.^[28] However, although hydrogen peroxide has been considered a “green” reagent due to its harmless reaction products, i.e. water and oxygen, a controversial discussion is lately rising. Hydrogen peroxide is corrosive, a strong oxidant, and, considering its entire life cycle, the production relies on a costly process that cannot be considered green in all stages.^[29–31] Thus, in this work we propose the use of glucose as harmless fuel for the degradation of aromatic compounds. The chemoenzymatic catalysis, that takes place within our nanoreactors, involves the in-situ transformation of glucose into hydrogen peroxide, which is immediately used for the efficient peroxidation of the pollutants

2. Results and Discussion

2.1. Synthesis and characterization of chemoenzymatic nanoreactors

The fabrication of chemoenzymatic nanoreactors entails the synthesis of imidazole-decorated SENs and the subsequent attachment of hemin molecules to the polymeric network of the those through metal-ligand coordination (**Scheme 1**). SENs were herein prepared using GOx as biocatalyst (detailed synthesis procedure in *Supplemental Information* and **Table S1**). **Table 1** showcases all the samples synthesized in this study

and the shell thicknesses of the respective nanogels. Importantly, we aimed at fabricating polymeric shells of few nanometers in order to minimize the diffusion limitations that might be caused by thick layers. The use of vinyl imidazole (VIm) in the *in-situ* polymerization reaction allowed the allocation of imidazole motifs all along the shell formed by the polymeric network (sample SEN_1). Moreover, the co-addition of carboxyethyl acrylamide (CEAAm) or aminopropyl methacrylamide (APMm) monomers to the polymerization triggered changes in the chemical nanoenvironment of the shell. Specifically, carboxylic acids (in SEN_2) or primary amines (in SEN_3) could potentially change the charge of the coordination sphere of the hemin and, thus, have an effect in the conformation, stability, and catalytic performance of the integrated nanoreactors. Further, nanogels with hydroxyethyl acrylamide (HEAAm), as only propagating monomer, were synthesized as control sample (SEN_4). Hence, according to Dynamic Light Scattering (DLS) measurements, enzyme nanogels with an average diameter range from ≈ 9.2 to ≈ 13.5 nm, which corresponds to a film thickness of ≈ 1.0 to ≈ 3.0 nm, were obtained (**Table 1** and **Figure S1**). Similar sizes were measured by Scanning Electron Microscopy (SEM) and Atomic Force Microscopy (AFM) (**Figure S2 and S3**, respectively). In addition, the presence of imidazole, carboxylic acid, and amino functional groups within the respective protein nanogels was confirmed by Z-potential measurements and Fourier-Transform Infrared Spectroscopy (FTIR) (**Table S2 and Figure S4**).



Scheme 1. Schematic representation of the synthesis procedure and the core-shell arrangement of the catalysts within the integrated nanoreactors (INR). Imidazole-modified single-enzyme nanogels (SENs) are synthesized from free GOx enzyme (*i*) and mixed with hemin chloride (*ii*) for the fabrication of INRs. The scheme depicts the relative location of the catalysts within the nanoreactor, namely the biocatalyst in the core and the hemin catalyst in the shell.

Table 1. Samples synthesized in this work and their shell thicknesses calculated from the hydrodynamic diameters measured by DLS.

Nanogel sample	Monomers	Enzyme	Shell Thickness (nm)
SEN_1	HEAAm, VIm	GOx	2.3
SEN_2	HEAAm, VIm, CEAAm	GOx	3.0
SEN_3	HEAAm, VIm, APMm	GOx	1.8
SEN_4	HEAAm	GOx	1.0

Integrated nanoreactors (INR) were fabricated by the addition of hemin chloride (molar excess of 100, $n_{\text{hemin}}:n_{\text{SEN}} = 100$) to SEN_1-4 enzyme nanogels, giving rise to the respective INR_1 to INR_4 nanoreactors (detailed synthesis procedure in *Supplemental Information*). The chemical composition of the respective hybrids was revealed using a

variety of spectroscopic characterization techniques such as Z-potential, Raman, FTIR, DLS, X-ray photoelectron spectroscopy (XPS), and UV-Vis spectroscopy.

The embedment of hemin molecules within the nanoreactors was evidenced by the decrease of the Z-potential of the nanoreactors with respect to the protein nanogel samples (**Table S2 and S3**). Also, the characteristic Raman D band of hemin is herein shifted to higher wavenumbers (from 1350 to 1380 cm^{-1} in free hemin and INR samples, respectively) and its intensity is significantly lowered compared to the G-band, indicating a change in the chemical environment of the hemin molecules (**Figure S5**). Furthermore, the presence of the characteristic infrared bands of hemin (710 and 1700 cm^{-1} corresponding to C-H bond of the pyrrole ring and C=O stretch of the -COOH hanging groups of hemin, respectively) in the INR samples, together with a significant shift of the infrared bands attributed to the terminal polyvinyl groups (from 1060 to 1028 cm^{-1}), evidenced the interaction of the polymer with hemin molecules (**Figure S6**).^[22] The presence of iron within the INR samples, including a small portion of Fe^{3+} (peak at 55 eV, 12 at% in **Figure 1A, Table S4 and Table S5**), was confirmed by XPS (**Figure S7**). Moreover, the analysis of N 1s region evidenced the N-Fe interaction and, thus, the presence of the pyrrolic ring within the network (**Figure S8**).

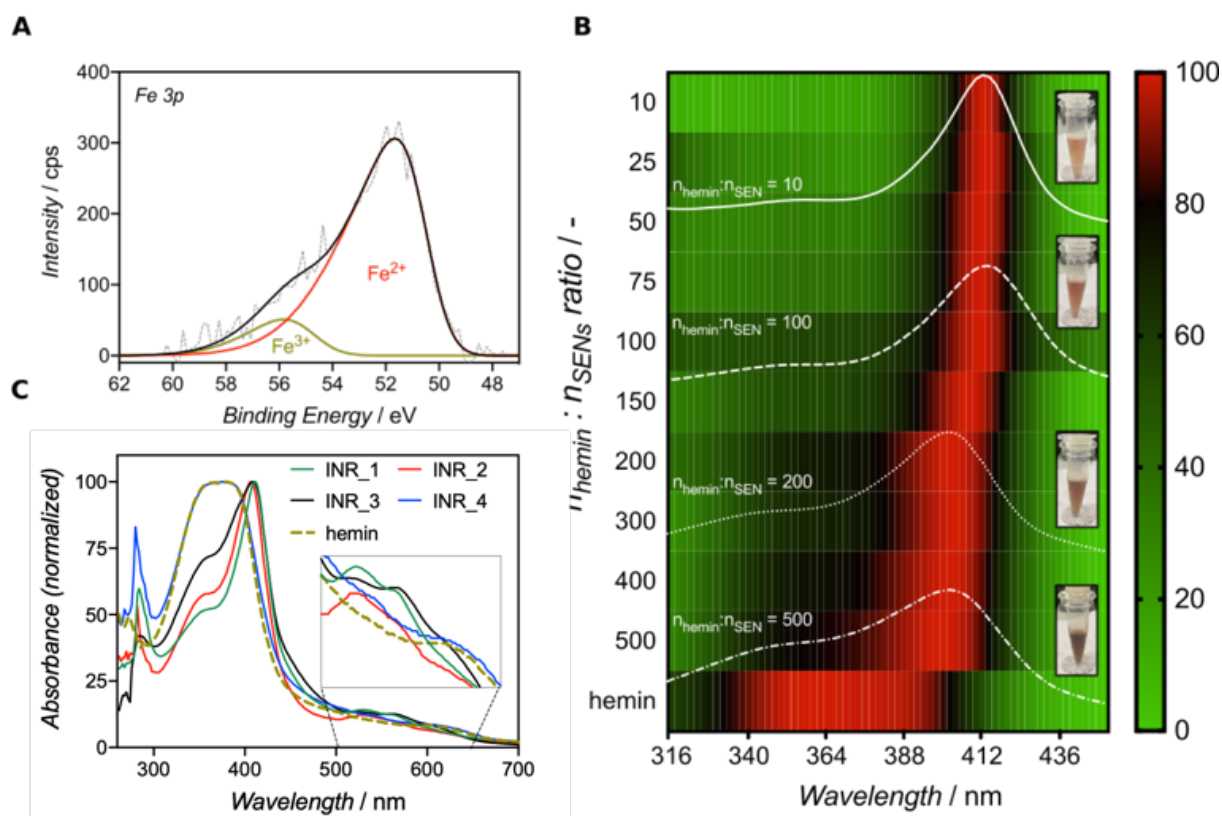


Figure 1. Spectroscopic analysis of INR samples. A) Fitted XPS spectrum of the Fe 3p component of the INR_1 sample. The Fe region is deconvoluted corresponding to Fe²⁺ and Fe³⁺ components. B) Scaled heat-map representation of the intensity of the UV-Vis spectra of INR_1 samples synthesized at a range of hemin:SEN molar ratios ($n_{\text{hemin}}:n_{\text{SEN}}$ from 10 to 500). The spectra of the samples prepared with a $n_{\text{hemin}}:n_{\text{SEN}}$ ratio of 10, 100, 200, and 500 are overlaid. Photographs of these solutions are shown as insets. C) UV-Vis spectra of INR samples in comparison to free hemin (non-continuous line). Spectra are zoomed in (5x) at the 500-650 nm spectral window in order to clearly appreciate the shift of the Q bands in the imidazole-coordinated samples.

As mentioned before, the peroxidation of the hemin catalyst is boosted when it is coordinated to imidazole ligands. This interaction can be visualized by UV-Vis spectroscopy by observing the shift of the characteristic Soret band of the hemin molecule.^[32] Indeed, this band is usually shifted to that of the hemin-histidine complex (400-415 nm range).^[33] Thus, UV-Vis absorption spectra were measured to further explore the interactions between hemin and the polymeric network within the INR samples. Hence, samples with $n_{\text{hemin}}:n_{\text{SEN}}$ ratios ranging from 10:1 to 500:1 were

synthesized and their UV-Vis spectra characterized. As observed from the UV-Vis intensity plot in **Figure 1B**, the samples prepared with $n_{\text{hemin}}:n_{\text{SEN}}$ ratios up to 150 (0.15 mg ml⁻¹ of hemin) showed very clean spectra with a maximum of the Soret band at 412 nm and a reddish solution. However, higher molar excess of hemin led to a gradual shift of the maxima of the Soret peak towards lower wavelengths (from 412 to 396 nm for a hemin excess of 150 and 500, respectively). Moreover, a band shoulder at 356 nm emerged in samples prepared with a $n_{\text{hemin}}:n_{\text{SEN}}$ ratio above 150, turning the samples brownish. Importantly, the bathochromic shift of the characteristic Soret band to higher wavelengths is only observed in imidazole-bearing nanogels (INR_1-3) (**Figure 1C**). In addition, the rise of low intensity satellite peaks of the Soret band (Q bands) at 533 and 565 nm (zoomed inset in **Figure 1C**) supports the hemin-imidazole interaction in INR_1, INR_2, and INR_3 samples.^[34] However, the comparison of UV-Vis spectra of imidazole-bearing samples showcased the influence of the chemical environment on the hemin-imidazole interaction in the integrated nanoreactors. The presence of carboxylic acids (INR_2) leads to a slight shift of the Soret peak by 2 nm (from 412 to 410 nm in INR_1 and INR_2 samples). Yet, the visible light absorption spectrum of the INR_3 sample, with amino groups contained in its structure, is significantly different. Besides the shift of a broader Soret band to 408 nm and a shift in the Q bands, we observed a shoulder at 390 nm which might indicate the presence of stacked hemin molecules. Contrastingly, the spectrum of the INR_4 sample fits with that obtained with free hemin. The detected maxima at 356 and 390 nm are assigned to hemin hydroxide monomers and μ -oxo bridged hemin dimer compounds, respectively.^[35]

We further characterized the sizes and morphologies of the hybrid nanoreactors by SEM, transmission electron microscopy (TEM), AFM, and DLS. SEM and TEM images of INR_1 nanoreactors suggested homogeneous and spherical particles with an average

size of 13.7 ± 1.8 nm (**Figure 2A and 2B and Figure S9 and Figure S10**). We confirmed the pseudo-spherical morphology of the integrated nanoreactors by high-resolution AFM (**Figure 2C**). Similar diameter sizes and shapes were found by SEM, AFM and DLS for INR_2 and INR_4 samples (**Figure S9, Figure S11 and Figure S12 and Table S6**). Yet, nanoreactors decorated with both imidazole and amino groups (namely, INR_3) showed completely different morphologies and dimensions. Indeed, the addition of hemin chloride to the SEN_3 sample triggered the aggregation of the individual nanogels. These particles could be recovered by centrifugation. We determined that a hemin excess of ≥ 400 was needed to achieve the complete recovery of the nanogels from solution and the formation of a brown precipitate (**Figure S13**). Under these conditions, SEM pictographs of INR_3 showed the formation of polydisperse particles with sizes from 100 nm to $> 1 \mu\text{m}$ (**Figure 2D and Figure S9**). Plus, high-resolution AFM images of the 100 nm sized particles suggested the presence of smaller units of $\approx 10\text{-}20$ nm, which likely correspond to assembled single enzyme nanogels (**Figure 2D, right, and Figure S11**).

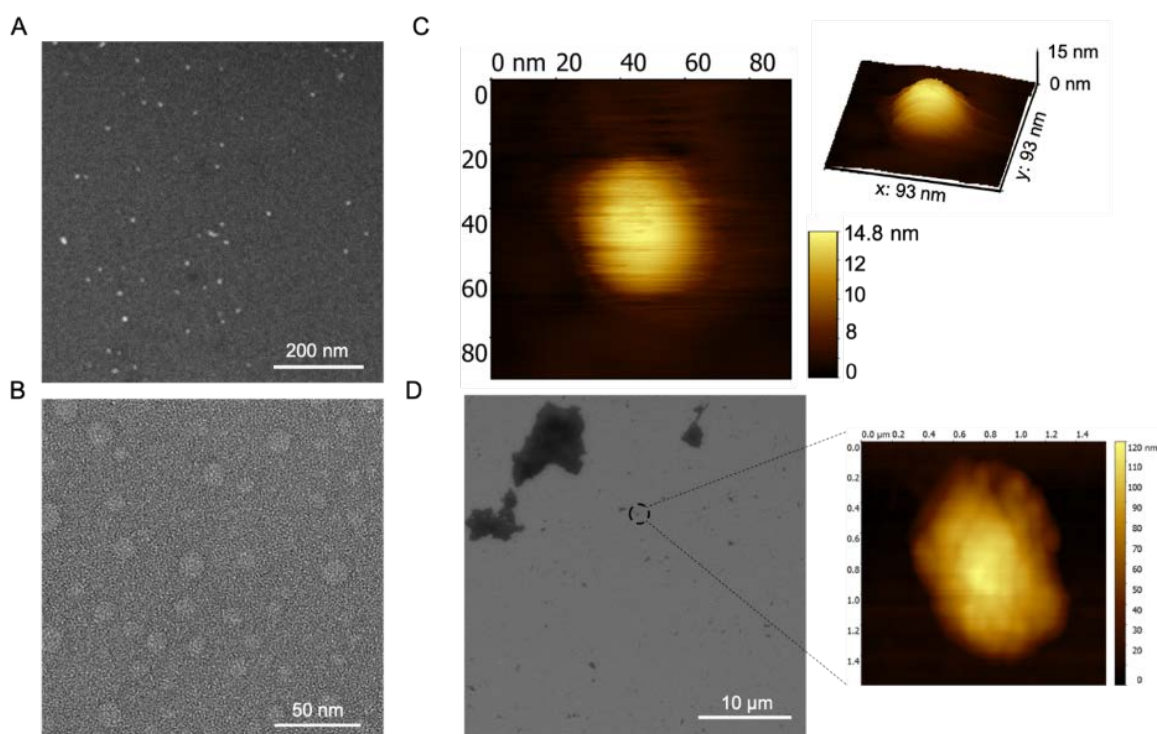


Figure 2. Structural characterization of the hybrid nanoreactors. Sample homogeneity and morphology of INR_1 was revealed by SEM (A), TEM (B), and high-resolution AFM (C). The inset image shows the 3D reconstruction of a single INR_1 particle. D) SEM pictograph of the INR_3 sample with a high-resolution AFM image of one of the small aggregates within the sample.

Thus, we have demonstrated a dual function of hemin molecule within the INR_3 hybrids. Besides providing the peroxidase-like functionality, hemin plays a structural role by triggering the assembly of the nanoreactors into heterogeneous chemoenzymatic catalysts. Such assembly might be driven by the interaction between the amino groups at the surface of the nanogel and the carboxylic acids of the hemin compound and further π - π stacking interactions between the hemin pyrrolic rings, as suggested by the emerged band at 390 nm in the INR_3 sample (**Figure 1C**).^[22] Compared to homogeneous chemoenzymatic catalysts (i.e. INR_1, INR_2, and INR_4), which can be dissolved/dispersed in the reaction media, the INR_3 heterogeneous catalyst is a recyclable system where the nanoreactors can be easily isolated from the products and reused through a simple rejuvenation process, as demonstrated in the following experiments.

2.2. Integrated chemoenzymatic catalysis

In this work, we aimed at synthesizing chemoenzymatic nanoreactors with high catalytic performance. As mentioned before, the coordination of hemin to imidazole ligands boosts the peroxidase-like activity of the catalyst. However, as the hemin molecules are allocated around the enzyme, the overload of those could block the polymeric pores and induce mass transfer issues within the nanoreactor, interfering with the enzymatic reaction that takes place in the core. Thus, an adequate $n_{\text{hemin}}:n_{\text{SEN}}$ ratio, that provides high peroxidation performance with low substrate diffusion issues, is sought for the sake of the cooperative chemoenzymatic reaction. Therefore, we tested sequential reactions with INR_1-4 samples synthesized at increased hemin loadings. Reactions were performed at a fixed nanoreactor concentration (16 nM) using glucose

(30 mM in sodium acetate 100 mM pH 6.0) and ABTS (1 mM) as substrates. The color change was monitored for each sample and their activity rates are plotted in **Figure 3A**. Noticeably, nanoreactors bearing imidazole groups, i.e. INR_1-3, improved the activity measured for the INR_4 sample by up to 800% in the assayed range. The low peroxidation activity found for INR_4 indicates an unspecific adsorption of hemin-hydroxide molecules to the polymeric network. Moreover, high loads of hemin (above a $n_{\text{hemin}}:n_{\text{SEN}}$ ratio of 400) led to a drop in the performance of the sequential reaction (**Figure 3B**). These features are also found when the peroxidase-like and glucose oxidase functionalities of the hybrids were tested independently (**Figure S14A and Figure S14B**, respectively), evidencing the peroxidation as the limiting step in the concurrent reaction. According to these activity profiles, we selected the $n_{\text{hemin}}:n_{\text{SEN}}$ ratio of 400 as the best condition found for the fabrication of nanoreactors with the highest catalytic performance. Therefore, this condition was used in this work for further catalytic characterization of the hybrid nanoreactors.

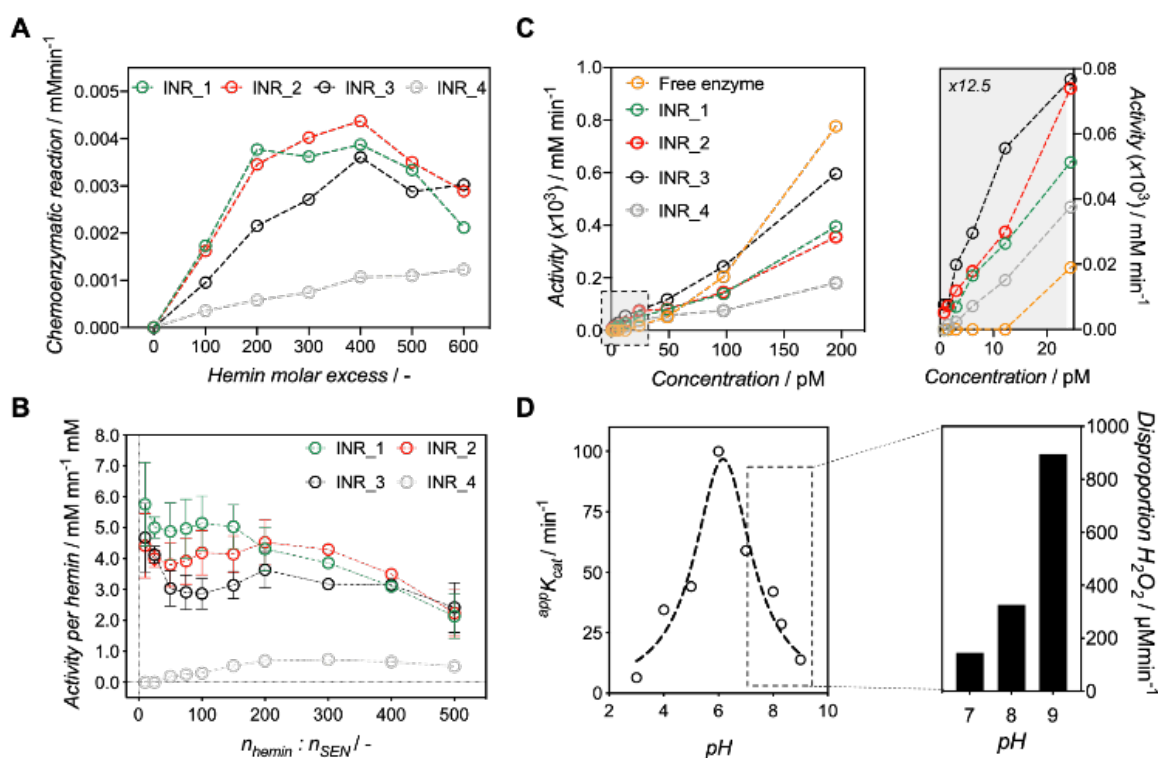


Figure 3. Activity plots of INR samples. A) One-pot chemoenzymatic activity tests of the nanoreactors synthesized with increasing hemin loads at same nanoreactor concentration (16

nM). B) Representation of the one-pot catalysis rates per mol of the organic catalyst. C) Activity plots of tandem reactions performed at very diluted conditions (0.7 to 200 pM of GOx). A zoomed-in plot is shown to appreciate the differences in the catalytic performance at GOx concentrations lower than 25 pM. D) pH-dependent activity profile of tandem chemoenzymatic catalysis of the INR_1 sample. Catalase-like activity of the nanoreactors at high pH is measured.

The measurement of the kinetic parameters corresponding to the one-pot reaction pointed out interesting features (**Table 2 and Figure S15 and Figure S16**). Surprisingly, the best catalytic efficiency was found for the heterogeneous catalyst INR_3, with a $^{app}k_{cat} / ^{app}K_m$ ratio of 364. Even though the aggregation of the nanoreactors triggers substrate diffusion limitations (V_{max} of 2.2 vs. 3.6 $\mu\text{M min}^{-1}$ and $^{app}k_{cat}$ of 270 vs. 317 min^{-1} measured for INR_3 and INR_1, respectively), the high affinity towards substrates as observed from the INR_3 sample ($^{app}K_m$ of 0.7 vs. 2.7 mM for INR_3 and INR_1, respectively) boosts its catalytic efficiency. Moreover, significantly lower apparent Michaelis constant values ($^{app}K_m$) were obtained, if compared to the free GOx/HRP one-pot reaction (0.7 to 2.7 vs. 31.9 mM for nanoreactor and free enzyme systems, respectively). This effect could be explained by the confinement effect of both catalysts within the nanoreactors.

Our core-shell system involves the arrangement of hemin molecules around the enzyme. Thus, the product of the enzymatic reaction is likely further transformed on its way to leave the nanoreactor through the hemin-decorated shell, increasing the overall performance of the cooperative reaction. This effect is clearly evidenced at highly diluted conditions. Despite showing lower catalytic performance than the free-enzyme system under the assayed conditions (364 vs. 817 $\text{min}^{-1}\text{mM}^{-1}$ for INR_3 and free enzyme system, respectively), the high efficiency of the cooperative reactions in colocalized and confined catalysts allowed us to detect the presence of glucose at concentrations lower than 20 pM (**Figure 3C**).

Table 2. Kinetic parameters measured for INR samples and the free GOx/HRP system ^{a)}

Sample	^{app} K _m (mM)	V _{max} (μM min ⁻¹)	^{app} k _{cat} (min ⁻¹)	^{app} k _{cat} / ^{app} K _m (min ⁻¹ mM ⁻¹)
INR_1	2.7±0.8	3.6±0.3	317±15	118
INR_2	1.4±0.3	3.2±0.2	370±25	265
INR_3	0.7±0.2	2.2±0.1	270±10	364
INR_4	1.2±0.4	1.2±0.2	54±2	45
GOx+HRP	32±7	20±4	26080±1910	817

^{a)} Reaction conditions: catalysts (concentration range 0-25 nM) and glucose (0-50 mM) are mixed in a reaction buffer (sodium acetate 100 mM pH 6.0) containing ABTS (1 mM) as chromogenic substrate. Activity is monitored at 416 nm.

Next, we analyzed the effect of the pH on the hemin-imidazole interaction within the INR samples and on their performance as tandem catalyst. We demonstrated that the hybrids are stable at a wide pH range (pH 5.0 to pH 9.0) (**Figure S17 A**) by measuring the UV-Vis spectra in different buffers. However, we observed that the performance of the nanoreactors was strongly dependent on the pH. The optimum conditions for the chemoenzymatic reaction were found to be pH 6.0 in 50 mM sodium acetate (**Figure 3D** and **Figure S17B**). Above pH 7.0, we observed a strong decrease of the activity. Since the glucose oxidase activity of the encapsulated GOx is almost constant up to pH 9.0,^[15] this loss of activity is likely to be related to the hemin catalyst. Moreover, we observed the presence of small bubbles in the reaction vessels at high pH that might indicate a new catalytic reaction occurring in the nanoreactors under the conditions in which the peroxidase-like activity of the hemin catalyst is nearly inactivated and therefore the hydrogen peroxide concentration is relatively high. This weak catalase-like activity of the nanoreactors was confirmed using a catalase colorimetric activity assay (InvitrogenTM) (**Figure 3D**). A similar effect has been found in some peroxidases at high hydrogen peroxide concentrations and basic pH values.^[36] On the other hand, the decrease of activity observed at pH < 5.0 might be related to cleavage of the Fe-imidazole bond due to the protonation of the coordinated imidazole ligands.^[25]

2.3. Stability of the hybrid nanoreactors

The ability of the hybrid nanoreactors to work in different reaction media is key for their application in the peroxidation of organic pollutants.^[37] We tested the ability of the nanoreactors to peroxidize 2,2'-azino-bis(3-ethylbenzothiazoline-6-sulfonic acid (ABTS) using glucose in presence of different organic solvents, such as isopropanol (iProp), acetonitrile (ACN), and dimethylformamide (DMF).

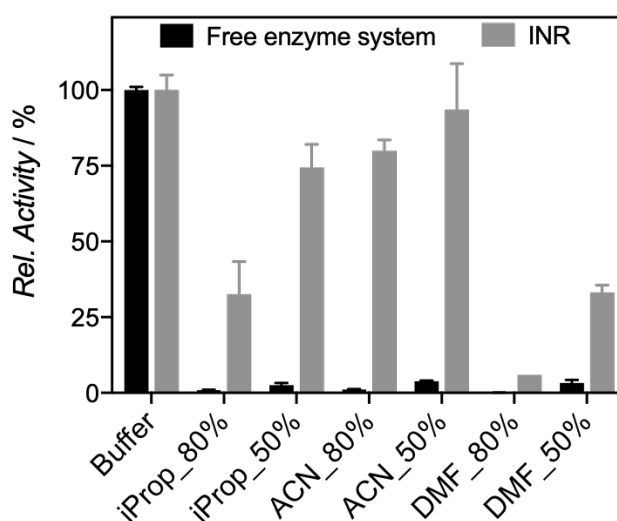


Figure 4. Activity chart showing the relative activity of hybrid nanoreactors and the free enzyme system in different solvent compositions. The activity in water is set as 100%.

As observable from **Figure 4**, the stabilizing effect of the polymeric scaffold is evident. Compared to the free enzyme system, which loses its ability to oxidize ABTS in organic solvents, the hybrid nanoreactors keep reasonably good activity in 50% (v/v) solutions of ACN and iProp, with $\geq 75\%$ of the activity retained, as measured in acetate buffer. Surprisingly, only $\approx 20\%$ of the activity was lost using 80% (v/v) ACN as co-solvent. In general, except for the case of DMF, we observed that the effect of the solvents in the encapsulated biocatalyst is moderate owing to the structural protection provided by the polymer (**Figure S18A**). Although to a lower degree, the hemin catalyst is also stabilized

within the polymeric network. This effect is especially observed when ACN is used as co-solvent (**Figure S18B**).

2.4. Removal of phenolic derivatives and dye pollutants

2.4.1. INR_3 nanoreactors are robust heterogeneous catalysts

Here, we propose a green approach for the degradation of dyes, in which harmless glucose is the only fuel used for the *in-situ* H₂O₂ production and subsequent degradation of phenolic derivatives and organic dyes. For this experiment, we utilized INR_3 because it has shown to be the nanoreactor with the highest catalytic turnovers and, being a heterogeneous catalyst, an efficient removal from the reaction solution is facilitated. We first tested its robustness and reusability as heterogeneous chemoenzymatic catalyst in sequential cyclic reactions and ON-OFF switching activity assay (**Figure 5A**).

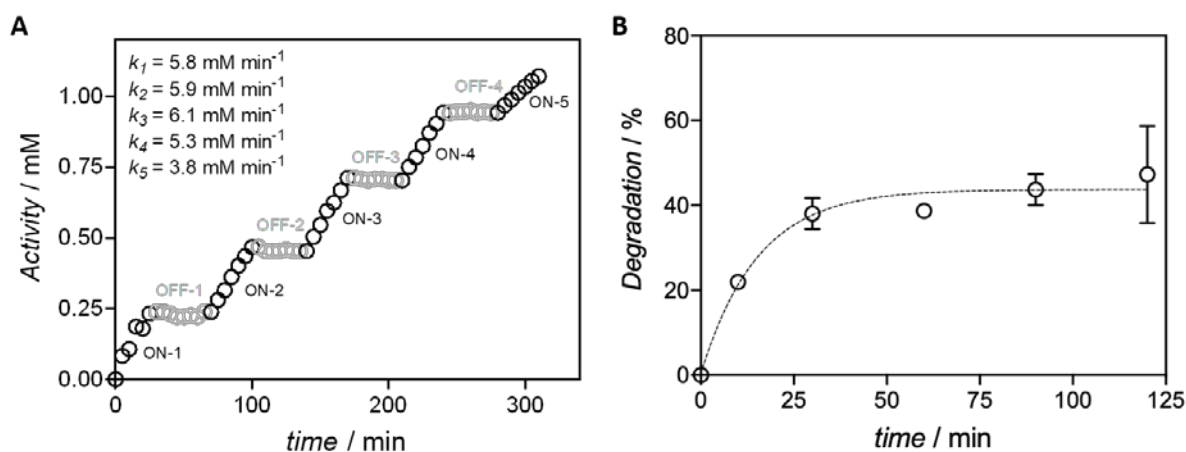


Figure 5. A) ON–OFF switching experiment in presence (ON) and absence (OFF) of the catalyst. B) Degradation yields, as %, of 1 mM of phenol and phenolic derivatives after 2 h of reaction time, using 0.6 μM of nanoreactors.

We started the reaction with the addition of INR_3 to a glucose/ABTS solution (ON phase) and stopped the reaction by centrifugation after 30 sec (OFF phase). This process was repeated 5 times to obtain 5 reaction cycles. The reaction stopped completely upon

the withdrawal of the catalyst, meaning a minimal loss of the catalyst over the cycles. Moreover, the catalytic rate of the nanoreactors derived from the slope of the curve in each ON cycle (k in **Figure 5A**) was constant for the first 3 cycles. Thereafter, the performance dropped by 12% and 47% in cycle 4 and 5, respectively. Consequently, the nanoreactors are efficiently (activity loss of < 15%) reused for up to 4 cycles.

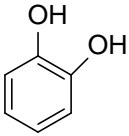
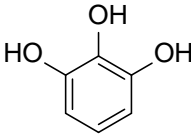
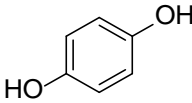
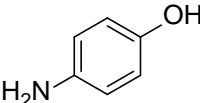
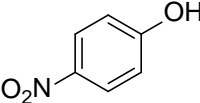
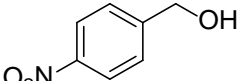
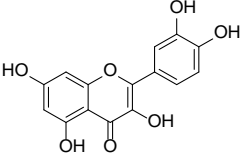
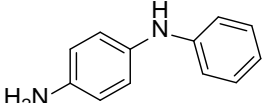
2.4.2. Test of the degradation potential of INR_3 sample

To the best of our knowledge, all reported biocatalyst-independent peroxidase-like systems to degrade organic compounds are based on the external addition of hydrogen peroxide. On the other hand, biocatalyst-driven systems, mostly HRP, are usually inactivated in the presence of high concentration of hydrogen peroxide.^[38] Thus, an alternative for the *in-situ* generation of hydrogen peroxide that is rapidly transformed to avoid *hot-spots* and the irreversible oxidative inactivation by H₂O₂ is sought.^[28] This issue has been partially sorted out or diminished by the combination of the peroxidase with polymers, i.e. polyethylene glycol or gelatin, which combination has shown increased stability of the enzyme.^[39] In this work, we present the GOx/hemin polymeric nanoreactors as a new and alternative system to the peroxidation of a broad number of organic compounds.

We tested the degradation potential of the nanoreactors using phenolic derivatives and glucose as the only fuel. First, the degradation rate of phenol was assayed using INR_3 nanoreactors. A concentration-dependent catalytic initial rate and a typical fast-then-slow catalytic profile was observed (**Figure 5B**). As observed in **Figure S19**, ~ 50% of phenol is degraded after 2 h of reaction using a catalyst concentration as low as 0.78 μM (which corresponds to 25 μg of GOx enzyme).

The ability of the nanoreactors to act over a broad number of phenolic derivatives would increase the impact of this system. Hence, we tested the degradation of a total of 8 more phenolic derivatives and 4 complex organic dyes. All reactions were carried out under the conditions described for phenol degradation (1 mM of phenolic derivative, 50 mM glucose, and 0.78 μ M of nanoreactors in a PBS/acetonitrile (50%, v/v) mixture). As collated in **Table 3**, a wide range of aromatic compounds could be degraded according to our results, with marked disparities in transformation efficiency. Thus, meta-substitutions of the phenol compound, i.e. catechol and pyrogallol, showed complete transformations, whilst the diphenolic compound hydroquinone showed the lowest degradation rate (22%) in this series. Therefore, the oxidation mechanism herein proposed seems to be less efficient for the formation of *p*-quinones. Moreover, medium-low degradation rates were observed when 4-nitrophenol (47%) and 4-benzyl alcohol (30%) compounds were tested. This effect can be explained by the presence of the NO₂-group, which electronic withdrawal reduces the reactivity of the aromatic ring.^[39] Further, high degradation values were also obtained for complex polyphenols such as quercetin compound or amino-modified aromatic rings (**Figure S20**).

Table 3. Chemical structures of assayed aromatic compounds and degradation efficiency (as %).

Compound	Catechol	Pyrogallol	Hydroquinone	4-aminophenol
Chemical Structure				
Degradation. %	100	100	22	95
Compound	4-nitrophenol	4-benzyl alcohol	Quercetin	N-phenyl-p-phenylenediamine
Chemical Structure				
Degradation. %	47	30	100	90

It has been reported that the direct addition of H₂O₂ (1 mM) to free peroxidase (HRP) shows very low phenol degradation rates (less than 10%) due to the inactivation of the catalyst unless the enzyme is protected by a polymeric mantel.^[40] Thus, the good degradation yields found in our system can be explained by the sheltered hemin catalyst and the progressive release of H₂O₂, which ensures a low concentration of the peroxide in solution. Hence, these results are comparable to other (chemo)enzymatic cascades with *in-situ* H₂O₂ production reported in the literature, yet the enzyme concentration is usually higher in those (e.g. 8 mg of peroxidase is needed for a maximum degradation of *p*-aminophenol of 50% after 7 h of reaction).^[38] Also, our system does not use expensive cofactors, i.e. NADH, and shows high efficiency and low concentrations and a broad substrate specificity.^[41,42] Therefore, we can state that, in addition to the protection given to the (bio)catalysts and the controlled release of H₂O₂, the confinement of the (bio)catalysts in small volumes, mimicking metabolic channels in cells, is a relevant feature that lead to efficient (degradation) reactions.

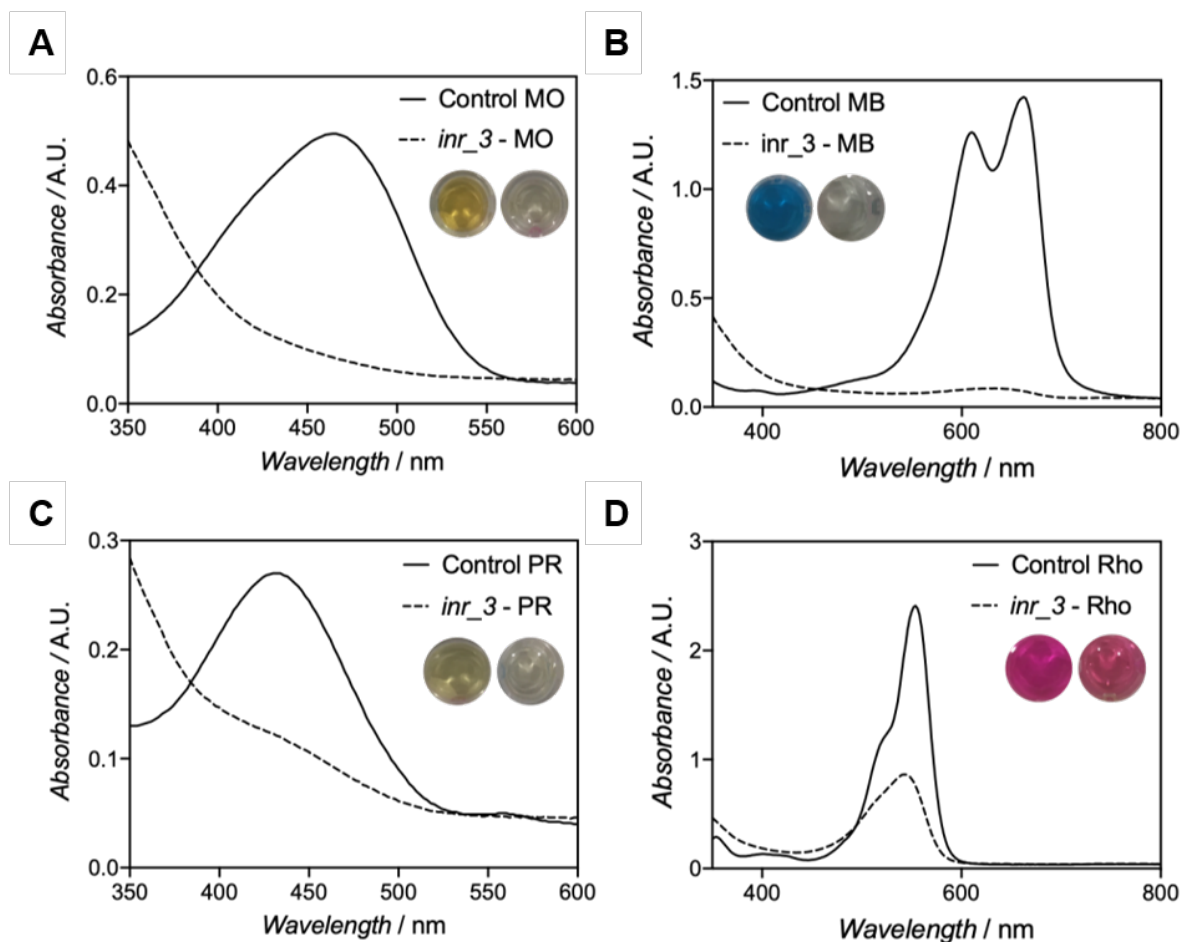


Figure 6. Degradation ability of INR_3. A-D) UV-Vis spectra of 50 μM of dyes (methyl orange, MO, in A; methylene blue, MB, in B; phenol red, PR, in C; and rhodamine B, Rho, in D) before (Control) and after overnight reaction (INR_3). Degradation experiments were performed using 100 nM of nanoreactors, 50 μM of dyes, and 50 mM of glucose at 42°C.

Motivated by the high degradation potential of the hybrids using small aromatics, we tested the ability of INR_3 to decolorize complex organic dyes using glucose as the only fuel. A first attempt was performed using 10 μM of methyl orange (MO), 50 mM of glucose and 50 nM of nanoreactors, yielding a $\sim 75\%$ of bleaching of the dye as measured by UV-Vis after 2 h reaction time (**Figure S21**). The rapid disappearance of the absorption at 466 nm suggests that the chromophores responsible for the typical orange color of MO are degrading. Further, almost 100% of degradation was achieved by increasing the nanoreactor concentration to 100 nM. These successful results persuaded us to test other organic dyes with different chemical structures. Thus, in contrast to anionic MO, we assayed cationic methylene blue (MB) and rhodamine B

(Rho), and phenol red (PR) as anionic and phenolic dye.^[43] Gratifyingly, almost complete degradation of MO, PR, and MB dyes, added as 10 μM solutions, was observed after 2 h of reaction time (**Figure S22**), and longer incubation times led to complete bleaching of those dyes at an even higher concentration of 50 μM (**Figures 6A-D**). Lower, but still acceptable degradation rates were obtained when Rho was used, with a maximum of 70% of degradation after overnight incubation.

3. Conclusion

We have described new integrated chemoenzymatic nanoreactors embedded in a porous and flexible polymeric scaffold. The advantageous assembly of the catalyst into a core-shell format, in which the biocatalyst is located in the core and the chemical catalyst, the hemin, in the shell, leads to a very efficient hybrid nanoreactor. Moreover, the immobilization of hemin molecules through the imidazole ligands of the polymeric mantle mimics the chemical environment of iron-porphyrin molecules in peroxidase enzymes. The preservation of the small size of the integrated nanoreactors limits diffusion issues and ensures a close positioning of both types of catalysts within the same nanounit. Moreover, we have changed the charge properties of the coordination sphere of the hemin by introducing amino groups and carboxylic acids to the polymeric network. Surprisingly, we observed that the presence of amino groups not only improves significantly the affinity of the nanoreactors towards the substrate, but also induces the self-assembly of the nanoreactors into large aggregates.

The catalytic characterization of integrated nanoreactors suggested the peroxidation as the reaction limiting step in our systems. Compared to free enzyme systems, the nanoreactors show a higher affinity and activity under diluted conditions, and noticeably higher stability in presence of organic solvents. Furthermore, there is a deep pH dependence of the performance of the nanoreactors, with a significant decrease of the

activity at pH below 5.0 and above 7.0. The decrease of activity at acidic pH can be explained by the protonation of the imidazole ligands within the nanoreactors. However, at basic pH, we have found that the peroxidase-like activity is gradually transformed into a weak catalase-like activity. Finally, we have confirmed the integrated hybrid nanoreactors as good candidates for environmentally benign transformation of recalcitrant pollutants using a glucose-fueled system in which the generation of hydrogen peroxide is controlled *in situ*. We foresee the use of this system for the chemoenzymatic concurrent reactions in which the intermediate product needs to be rapidly transformed to avoid inactivation issues of the (bio)catalysts.

Conflicts of interest

There are no conflicts to declare

Acknowledgements

This project has received funding from the Spanish Ministry of Economy and Competitiveness (MINECO) and FEDER funds in the frame of “*Plan Nacional – Retos para la Sociedad*” call with the grant reference MAT2017-88808-R. This work was performed under the Maria de Maeztu Units of Excellence Programme - MDM-2016-0618. A. B. thanks the Spanish Research Agency (AEI) for the funds within Ramón y Cajal program. A.R-A. thanks the Basque Government for his PhD fellowship. M.K. acknowledges financial support by the Spanish Ministry of Economy and Competitiveness (MINECO) within grant agreement no. MAT2016-77393-R, including FEDER funds.

References

- [1] P. N. R. Vennestrøm, C. H. Christensen, S. Pedersen, J. D. Grunwaldt, J. M. Woodley, *ChemCatChem* **2010**, 2, 249–258.

- [2] X. Wang, C. Hou, W. Qiu, Y. Ke, Q. Xu, X. Y. Liu, Y. Lin, *ACS Appl. Mater. Interfaces* **2017**, *9*, 684–692.
- [3] J. H. Schrittwieser, F. Coccia, S. Kara, B. Grischek, W. Kroutil, N. D'Alessandro, F. Hollmann, *Green Chem.* **2013**, *15*, 3318–3331.
- [4] H. C. Hailes, P. A. Dalby, J. M. Woodley, *J. Chem. Technol. Biotechnol.* **2007**, *82*, 1063–1066.
- [5] Y. Lin, L. Wu, Y. Huang, J. Ren, X. Qu, *Chem. Sci.* **2015**, *6*, 1272–1276.
- [6] C. A. Denard, J. F. Hartwig, H. Zhao, *ACS Catal.* **2013**, *3*, 2856–2864.
- [7] A. C. Marr, S. Liu, *Trends Biotechnol.* **2011**, *29*, 199–204.
- [8] M. Filice, J. M. Palomo, *ACS Catal.* **2014**, *4*, 1588–1598.
- [9] F. Rudroff, M. D. Mihovilovic, H. Gröger, R. Snajdrova, H. Iding, U. T. Bornscheuer, *Nat. Catal.* **2018**, *1*, 12–22.
- [10] Z. C. Litman, Y. Wang, H. Zhao, J. F. Hartwig, *Nature* **2018**, *560*, 355–359.
- [11] X. Li, Y. Cao, K. Luo, Y. Sun, J. Xiong, L. Wang, Z. Liu, J. Li, J. Ma, J. Ge, et al., *Nat. Catal.* **2019**, *2*, 718–725.
- [12] R. J. R. W. Peters, I. Louzao, J. C. M. Van Hest, *Chem. Sci.* **2012**, *3*, 335–342.
- [13] Z. Chen, H. Cao, T. Tan, *New J. Chem.* **2019**, *43*, 8517–8526.
- [14] A. Beloqui, S. Baur, V. Trouillet, A. Welle, J. Madsen, M. Bastmeyer, G. Delaittre, *Small* **2016**, *12*, 1716–1722.
- [15] A. Beloqui, A. Y. Kobitski, G. U. Nienhaus, G. Delaittre, *Chem. Sci.* **2018**, *9*, 1006–1013.
- [16] A. Rodriguez-Abetxuko, M. C. Morant-Minana, M. Knez, A. Beloqui, *ACS Omega* **2019**, *4*, 5172–5179.
- [17] A. Rodriguez-Abetxuko, M. C. Morant-Miñana, F. López-Gallego, L. Yate, A. Seifert, M. Knez, A. Beloqui, *Adv. Funct. Mater.* **2018**, *28*, 1803115.

- [18] A. Rodriguez-Abetxuko, D. Sánchez-deAlcázar, A. L. Cortajarena, A. Beloqui, *Adv. Mater. Interfaces* **2019**, *6*, 1900598.
- [19] S. Li, L. Zhang, Y. Jiang, S. Zhu, X. Lv, Z. Duan, H. Wang, *Nanoscale* **2017**, *9*, 16005–16011.
- [20] W. Jiang, X. Wang, J. Chen, Y. Liu, H. Han, Y. Ding, Q. Li, J. Tang, *ACS Appl. Mater. Interfaces* **2017**, *9*, 26948–26957.
- [21] Q. Wang, Z. Yang, M. Ma, C. K. Chang, B. Xu, *Chem. - A Eur. J.* **2008**, *14*, 5073–5078.
- [22] Y. Zhang, C. Xu, B. Li, *RSC Adv.* **2013**, *3*, 6044–6050.
- [23] W. Wu, Q. Wang, J. Chen, L. Huang, H. Zhang, K. Rong, S. Dong, *Nanoscale* **2019**, *11*, 12603–12609.
- [24] R. Qu, L. Shen, Z. Chai, C. Jing, Y. Zhang, Y. An, L. Shi, *ACS Appl. Mater. Interfaces* **2014**, *6*, 19207–19216.
- [25] E. Gkaniatsou, C. Sicard, R. Ricoux, L. Benahmed, F. Bourdreux, Q. Zhang, C. Serre, J. P. Mahy, N. Steunou, *Angew. Chemie - Int. Ed.* **2018**, *57*, 16141–16146.
- [26] B. Jiang, Y. Yao, R. Xie, D. Dai, W. Lu, W. Chen, L. Zhang, *Appl. Catal. B Environ.* **2016**, *183*, 291–297.
- [27] H. Babich, D. L. Davis, *Regul. Toxicol. Pharmacol.* **1981**, *1*, 90–109.
- [28] B. Burek, S. Bormann, F. Hollmann, J. Bloh and D. Holtmann, *Green Chem.*, **2019**, *21*, 3232–3249.
- [29] S. Z. Ismail, M. M. Khandaker, N. Mat and A. N. Boyce, *J. Agron.*, **2015**, *14*, 331–336.
- [30] K. Giddey, M. Kidd., T.J. Britz, G.O. Sigge and C. Lamprecht, *J. Appl. Environ. Microbiol.*, **2015**, *3*, 49–57.

- [31] A. Baker, Is Hydrogen Peroxide Actually a ‘Green’ Reagent?, can be found under <https://communities.acs.org/community/science/sustainability/green-chemistry-nexus-blog/blog/2016/08/18/is-hydrogen-peroxide-actually-a-green-reagent>, **2016**
- [32] Q. Liu, H. Wang, X. Shi, Z. G. Wang and B. Ding, *ACS Nano*, **2017**, *11*, 7251–7258.
- [33] Q. Wang, Z. Yang, X. Zhang, X. Xiao, C. K. Chang and B. Xu, *Angew. Chemie - Int. Ed.*, **2007**, *46*, 4285–4289.
- [34] R. Qu, H. Shi, R. Wang, T. Cheng, R. Ma, Y. An and L. Shi, *Biomater. Sci.*, **2017**, *5*, 570–577.
- [35] H. Shi, Y. Liu, R. Qu, Y. Li, R. Ma, Y. An and L. Shi, *Colloids Surfaces B Biointerfaces*, **2019**, *174*, 352–359.
- [36] P. Campomanes, U. Rothlisberger, M. Alfonso-Prieto and C. Rovira, *J. Am. Chem. Soc.*, **2015**, *137*, 11170–11178.
- [37] A. Schmid, J. S. Dordick, B. Hauer, A. Kiener, M. Wubbolts and B. Witholt, *Nature*, **2001**, *409*, 258–268.
- [38] J. Rocha-Martin, S. Velasco-Lozano, J. M. Guisán and F. López-Gallego, *Green Chem.*, **2014**, *16*, 303–311.
- [39] K-S. Ju and R.E. Parales, *Microbiol. Biol. Rev.*, **2010**, *2*, 250–272
- [40] S. Liu, B. Huang, G. Zheng, P. Zhang, J. Li, B. Yang, Y. Chen and L. Liang, *Intl J Biological Macromolecules*, **2020**, *150*, 814–822
- [40] V. A. Cooper and J. A. Nicell, *Water Res.*, **1996**, *30*, 954–964.
- [41] D. Jung, C. Streb and M. Hartmann, *Microporous Mesoporous Mater.*, **2008**, *113*, 523–529
- [42] D. I. Perez, M. M. Grau, I. W. C. E. Arends and F. Hollmann, *Chem. Commun.*, **2009**, 6848–6850
- [43] Y. H. Chiu, T. F. M. Chang, C. Y. Chen, M. Sone and Y. J. Hsu, *Catalysts*, **2019**, *9*, 430–462.

Supporting Information

Supporting Information is available from the Wiley Online Library or from the author.

Received: ((will be filled in by the editorial staff))

Revised: ((will be filled in by the editorial staff))

Published online: ((will be filled in by the editorial staff))